Environmental Earth Sciences (2025) 84:464
https://doi.org/10.1007/s12665-025-12455-2

ORIGINAL ARTICLE

Carbon capture and storage (CCS): CO2 basaltic mineralization through the phase transition from gas-solid to aqueous under low reaction kinetics

Amir Hossein Mazaheri[1] · Mohd Ridha Muhamad[1,2] · Muhammad Khairi Faiz[1] · Farazila Yusof[1,2] · Meor Faisal Zulkifli[1] · Zahiruddin Fitri Abu Hassan[3] · Hijaz Kamal Hasnan[4] · Omeid Rahmani[5] · Asefeh Asemi[6]

Received: 6 February 2025 / Accepted: 19 July 2025

Abstract

Advances in carbon capture and storage (CCS) technologies are being increasingly pursued as a means of diminishing the impact of anthropogenic CO_2 emissions. Mineral carbonation (MC) offers a promising approach to CO_2 mitigation by converting CO_2 into stable carbonates using natural minerals like basalt. This study investigates the feasibility of carbonation of Segamat basalt, focusing on the transition from gas-solid to aqueous phase under low reaction conditions. A comprehensive experimental approach evaluated the impact of particle size, temperature, reaction duration, liquid-to-solid ratio, and salinity on the carbonation efficiency of each metal oxide and overall CO_2 uptake. The results indicated that significant carbonation up to 71% for calcium can still be achieved with larger particle sizes, low temperatures, and low mechanical activation in the presence of adequate saline water. This finding implies the feasibility of industrial-scale MC with reduced energy consumption. By utilizing basalt feedstock as a plenteous and reachable natural resource, this research provides valuable insights into optimizing ex-situ MC processes and contributes to sustainable CO_2 sequestration strategies.

Keywords Mineral carbonation · Carbon capture and storage · Aqueous carbonation · Basalt · CO_2 sequestration

✉ Mohd Ridha Muhamad
ridha@um.edu.my

✉ Meor Faisal Zulkifli
meor@um.edu.my

Amir Hossein Mazaheri
amirh.mazaheri@gmail.com

Muhammad Khairi Faiz
mkhairifaiz@um.edu.my

Farazila Yusof
farazila@um.edu.my

Zahiruddin Fitri Abu Hassan
zahiruddin@um.edu.my

Hijaz Kamal Hasnan
hijazzains@um.edu.my

Omeid Rahmani
omeid.rahmani@soran.edu.iq

Asefeh Asemi
asemi.asefeh@uni-corvinus.hu

[1] Department of Mechanical Engineering, Faculty of Engineering, University of Malaya, Kuala Lumpur 50603, Malaysia

[2] Centre of Advanced Manufacturing and Material Processing (AMMP Centre), University of Malaya, Kuala Lumpur 50603, Malaysia

[3] Department of Building Surveying, Faculty of Built Environment, University of Malaya, Kuala Lumpur 50603, Malaysia

[4] Department of Geology, Faculty of Science, University of Malaya, Kuala Lumpur 50603, Malaysia

[5] The UK Global Talent – Exceptional Promise (Endorsed by the Royal Academy of Engineering), Edinburgh EH21 7LH, Scotland, UK

[6] Department of Information Systems, Institute of Data Analytics and Information Systems, Corvinus University of Budapest, Fővám tér 13-15, Budapest 1093, Hungary

Published online: 02 August 2025

Introduction

The atmospheric CO_2 level has increased significantly since the Industrial Revolution due to anthropogenic activities, including fossil fuel combustion and deforestation. The increase in CO_2 concentration (i.e., >400 ppm), along with other greenhouse gases (GHGs), is a significant factor in global warming and climate change. The dependence of large industries, power plants at the top of them, on burning fossil fuels for energy supply has significantly increased anthropogenic CO_2 emissions in the last century (Crippa et al. 2020; Ritchie et al. 2020). Contemporarily, this issue will not be removed by itself, as the International Energy Agency (IEA) has reported an average annual growth rate of 0.7% in global energy demand in the coming years (IEA 2023).

The global climate crisis has sparked a search for ways to tackle this problem and mitigate the effects of CO_2 emissions over the last decades. Several alternatives have been proposed in this regard, including the development of energy-efficient technologies and the increased use of renewable energy resources to reduce the reliance on fossil fuels (Bachu et al. 2007; Rafiee et al. 2018). A growing interest in the development of innovative carbon capture and storage (CCS) technologies is noticeable and can help mitigate the disastrous effects of greenhouse gas emissions (Kashim et al. 2020; Rahmanihanzaki and Hemmati 2022), aiming to limit global temperature increment to 1.5 degrees Celsius by 2025. Storage projects can target a capacity of approximately 700 million tons per annum (Mtpa) of CO_2 uptake. In other words, prognostications indicate that CCS technology can sequester around one-sixth of emitted CO_2 by 2050 (IEA 2021). One such technology that has garnered significant attention in recent years is mineral carbonation (MC), also referred to as carbon mineralization (Benson and Surles 2006; Park et al. 2016; Tan et al. 2021). Since there are abundant and widely accessible feedstocks for MC, CO_2 can be safely and permanently stored in this manner (Mazzotti et al. 2005; Romanov et al. 2015). This process involves the reaction of CO_2 with metal oxides found in natural minerals and industrial wastes to form stable carbonates (Luo and He 2021; Yadav and Mehra 2021).

Alkaline-bearing mine residues, such as wollastonite, serpentinite, peridotite, and olivine can produce gigaton-scale amounts of stable carbonates per year (Kelemen et al. 2011; Kwon et al. 2011; Gadikota et al. 2014; Dichicco et al. 2015; Rahmani et al. 2016; Yadav and Mehra 2019; Wang and Dreisinger 2023). Basalt is a volcanic rock commonly found in the Earth's crust. It contains silicon (Si), iron (Fe), calcium (Ca), sodium (Na), potassium (K), magnesium (Mg), and aluminum (Al) oxides, making it a suitable natural MC feedstock (Matter et al. 2011; Marieni et al. 2021; Liu et al. 2022; de Obeso et al. 2023). Research on the mineral carbonation of basalts indicates that most studies are categorized as aqueous MC, focusing on evaluating the in-situ MC capacity of basalt sites (Grover and Baldock 2012; Kumar et al. 2017; Snaebjornsdottir et al. 2017; Wells et al. 2017; Callow et al. 2018; Kumar and Shrivastava 2019a; Liu et al. 2019, 2022; Marieni et al. 2021; de Obeso et al. 2023). By comparing the chemical compositions of basalts from various sources, it can be concluded that although the amount of each component may differ among the different basalts, the effect of these components remains relatively constant. This consistency facilitates the comparison of the results from pulverized basalts in ex-situ MC. Because the porosity volume of basalt samples is very substantial for evaluating CO_2 sequestration capacity in in-situ MC, it varies for each basalt type. However, this barrier is removed when the goal is to examine ex-situ MC of basalt powder, making the data more comparable.

Further, the reaction rate is raised by increasing the surface area of feasible feedstock (Garcia et al. 2010) in CO_2 mineralization. That is why most studies have mainly focused on fine particles less than 200 µm, leading to an elevated rate of carbonation in high temperatures and high pressures (Werner et al. 2013; Gadikota et al. 2014; Yadav and Mehra 2017; Liu et al. 2018; Li et al. 2019). Producing fine powders in large quantities poses significant practical challenges, particularly for industrial-scale applications. Additionally, using high temperatures or pressures means more energy consumption, which undermines the MC's primary role in achieving the net-zero emissions goal. Besides, the feasible elements within a feedstock, like basalt, need a dissolution medium to interact with CO_2-rich water in the inducted feedstock. Ayub et al. (2020) reported that the carbonation rate of basaltic samples, rich in feasible elements of Ca, Mg, and Fe, is increased in the presence of water. As a result of the dissolution process, these divalent cations are released to react with carbon dioxide and form solid carbonates.

Furthermore, it is necessary to understand the dynamics of carbonation reactions in an aqueous environment. Considering aqueous and gas-solid phases, the carbonation reaction for calcium and magnesium oxides, as well as calcium, magnesium, and iron silicates, can be presented as follows (Yadav and Mehra 2017; Rahmani 2020; Reynes et al. 2021):

$$H_2O + CO_2 \rightarrow H_2CO_3 \quad (1)$$

$$H_2CO_3 \rightarrow HCO_3^- + H^+ \quad (2)$$

$$HCO_3^- \rightarrow CO_3^{2-} + H^+ \quad (3)$$

$$(CaO\ or\ MgO) + 2\ H^+ \rightarrow (Ca^{2+}\ or\ Mg^{2+}) + H_2O \quad (4)$$

$$(Ca, Mg, Fe)_2SiO_4 + 4\ H^+ \rightarrow 2(Ca^{2+}, Mg^{2+}, Fe^{2+}) + SiO_2 + 2H_2O \quad (5)$$

$$(Ca^{2+}, Mg^{2+}, Fe^{2+}) + H_2O \rightarrow (Ca(OH)^+, Mg(OH)^+, Fe(OH)^+) + H^+ \quad (6)$$

$$(Ca^{2+}, Mg^{2+}, Fe^{2+}) + HCO_3^- \rightarrow (CaCO_3, MgCO_3, FeCO_3) + H^+ \quad (7)$$

$$(Ca^{2+}, Mg^{2+}, Fe^{2+}) + CO_3^{2-} \rightarrow (CaCO_3, MgCO_3, FeCO_3) \quad (8)$$

In gas-solid carbonation, CO_2 reacts directly with solid feedstocks that are less complex. The reactions below are also presented for three dissimilar categories (Gupta and Fan 2002; Fagerlund et al. 2009; Kale et al. 2012; Montes-Hernandez et al. 2012):

$$(CaO\ or\ MgO)_{(s)} + CO_{2(g)} \rightarrow (CaCO_3\ or\ MgCO_3)_{(s)} \quad (9)$$

$$(Ca(OH)_2 or Mg(OH)_2)_{(s)} + CO_{2(g)} \rightarrow (CaCO_3 or MgCO_3)_{(s)} + H_2O_{(l/g)} \quad (10)$$

$$(CaSiO_3 or MgSiO_3)_{(s)} + CO_{2(g)} \rightarrow (CaCO_3 or MgCO_3)_{(s)} + SiO_{3(s)} \quad (11)$$

By understanding the dynamics of carbonation reactions and adjusting the reaction variables, optimized conditions can be identified that accelerate the transformation into carbonated minerals, enabling carbonation reactions within a reasonable time (Shi et al. 2016; Tam et al. 2016).

In this study, the Segamat basalt samples, sourced from Johor, Malaysia, are selected as suitable feedstock for CO_2 mineralization because of their substantial alkaline content and favorable mineralogical characteristics (Ayub et al. 2020). With this, the feasibility of using a wide range of particles for CO_2-basaltic mineralization is investigated, considering the reduction in energy consumption and costs associated with low reaction conditions. A comprehensive experimental approach is employed to evaluate the carbonation efficiency of Segamat basalt across different particle sizes. By examining carbonation during the transition from a gas-solid to an aqueous phase, this study also aims to contribute valuable data to optimizing MC processes. The findings are expected to have significant implications for the practical application of MC in CO_2 sequestration, providing a potential pathway for large-scale CO_2 mitigation efforts using naturally abundant and readily available basalt samples.

Materials and methods

Segamat basalt samples

Basaltic samples required for CO_2 mineralization were collected from the Segamat site in Johor, Malaysia (Fig. 1). As an ultramafic rock, the Segamat basalt is ideal for CO_2

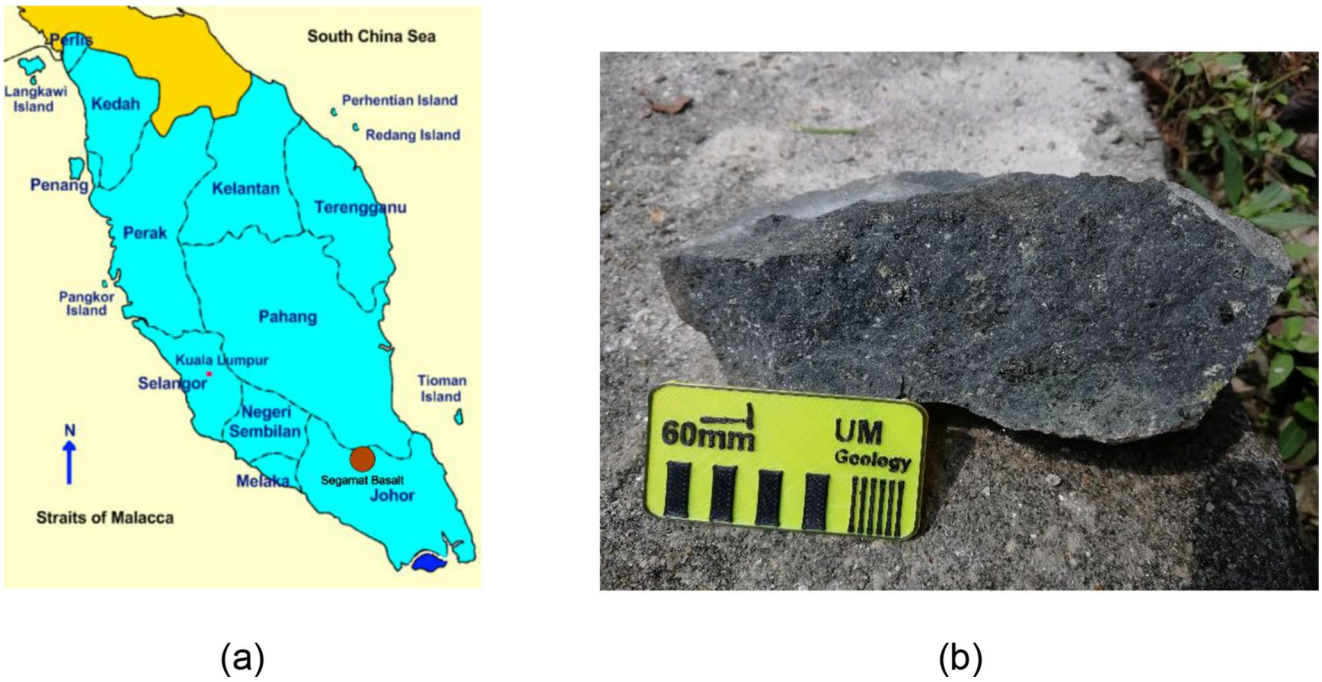

Fig. 1 (**a**) A locational map of the Segamat basalt in Peninsular Malaysia and (**b**) a basalt rock sample

mineralization due to its significant metal oxide content (Ayub et al. 2020; Yusoff et al. 2025).

Although fine grains (i.e., <200 µm in size) are more suitable for attaining higher degrees of carbonation, producing fine powder in large quantities for industrial MC applications can be a potential barrier to the development of CCS technology. Therefore, this study aimed to investigate bigger particles as well. The samples were crushed to produce a wide range of particle sizes. After sieving basalt powder through apertures of 212, 425, and 600 µm, the samples were divided into P1, P2, and P3 groups, corresponding to fine, mid-range, and coarse particles, respectively. The particle size distribution of each group was analyzed by Malvern Panalytical Mastersizer 2000.

Characterization measurements

Elemental characteristics of the Segamat basalt were determined by X-ray fluorescence (XRF) analysis, a versatile analytical technique used for the qualitative and quantitative determination of samples' elemental composition. For this purpose, seven samples from three particle size groups were analyzed using an XRD Rigaku Supermini 200 with a 50 kV −200 W Pd-anode X-ray source in a helium atmosphere.

Furthermore, X-ray diffraction (XRD, Rigaku MiniFlex 600) analysis, utilizing a Cu-Kα X-ray source with a 40 kV/15 mA power setting to generate radiation with a wavelength of 1.54 Å, was employed to investigate the crystal structure of the Segamat basalt samples before and after carbonation. XRD is a powerful technique for characterizing the crystalline structure of samples, providing valuable information about the atomic arrangement within the crystal lattice by irradiating a sample with X-rays and measuring the angles and intensities of the diffracted beams. The Segamat basalt samples were scanned from 5° to 65° (2θ) at a scan rate of 2°/min.

Moreover, a thermogravimetric analysis (TGA, Rigaku STA812 simultaneous thermal analyzer) was recruited to measure the weight loss of the Segamat basalt samples between 150 °C and 1000 °C. The TGA analysis was conducted in a nitrogen atmosphere with a 300 mL/min gas flow rate and 10 °C/min heating rate. The samples' weight loss was derived from CO_2 extraction resulting from the decomposition of carbonate minerals (Kashim et al. 2020). Therefore, the CO_2 weight% in the samples was represented by their weight loss in this temperature interval, which was used to calculate carbonation efficiency and CO_2 sequestration rate. A derivative thermogravimetry (DTG) was also used to provide a precise overview of the Segamat basalt samples' behavior during pyrolysis. Studying the DTG curve's peaks in different decomposition events can facilitate the identification and quantification of the multiple stages of thermal degradation. In addition, field-emission scanning electron microscopy (FESEM, ZEISS AURIGA) was used to analyze the Segamat basalt samples' microstructure, morphology, and surface roughness. By FESEM, a non-image of the Segamat basalt samples' surface was generated in higher quality.

Experimental apparatus

A reactor chamber was designed based on the principal parameters affecting the MC, including heating control, temperature measurement, vacuum system, CO_2 flow control, pressure measurement, agitation mechanism, and rotation speed control. These parameters were adapted from the literature (Luo and He 2021; Yadav and Mehra 2021) to facilitate this study, with more emphasis on thermo-mechanical activation and acceleration of carbonation reactions.

Based on the requirements, a 5-liter cylindrical reactor chamber was fabricated and utilized for the MC experiments. A heating element was positioned at the bottom of the chamber, as shown in Fig. 2. A speed control gearmotor was indirectly mounted to the stirrer shaft to provide stirring at desired speeds. The stirrer blades were designed so as to have efficient agitation in both polar and vertical axes and facilitate heat transfer from the bottom of the chamber to the feedstock. Although the system is mechanically capable of operating at high temperatures and pressures, the working temperature and pressure of the system were limited to 125 °C and 750 kPa according to the operating range of the selected sensors. A single-stage rotary vane vacuum pump was used to remove the air from the reactor chamber before starting the experiment. The control circuit monitors the sensors' data and controls the heating element and solenoid valve to keep the temperature and CO_2 pressure steady during the experiments. Figure 2 demonstrates a schematic of the MC system for CO_2 mineralization of the Segamat basalt samples in this study.

Experimental procedure

From the literature, five factors affecting the MC experiments were investigated: reaction temperature, reaction time, particle size, liquid-to-solid ratio (*L/S*), and salinity. Before beginning the experiments, air was vacuumed until the pressure reached 15 to 10 kPa. Then, pure CO_2 was injected into the chamber to raise the pressure to atmospheric levels for aqueous experiments and up to 250 kPa for gas-solid experiments. In doing so, the CO_2 purity remained at least 85–90% during the carbonation process according to the ideal gas law. The stirring speed was set to 60 RPM for all the experiments to avoid interfering with other parameters and to assess the feasibility of MC using

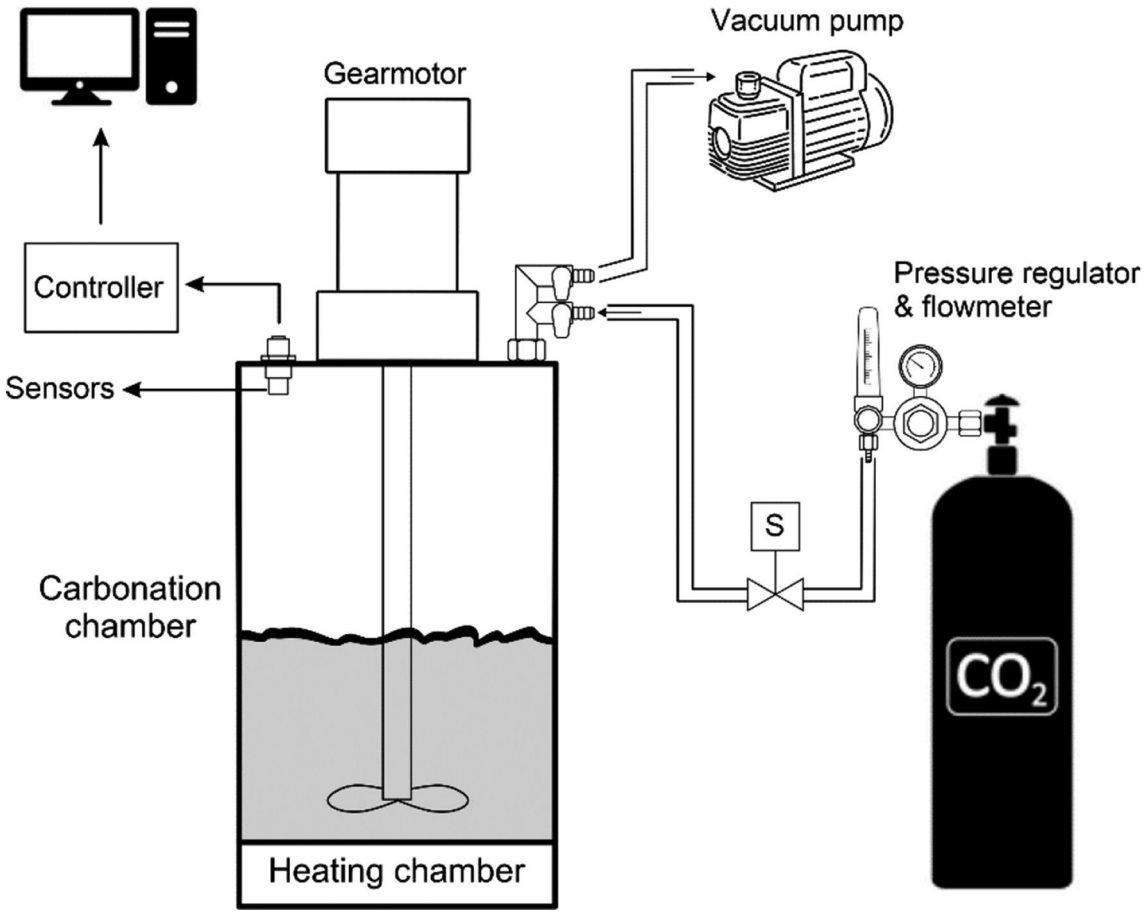

Fig. 2 A schematic of the MC system used for CO_2 mineralization of the Segamat basalt samples

a low-speed mechanical activation. The experiments were conducted in three phases: dry, transition, and aqueous. In this research, the transition phase is defined as a phase in which the amount of water is less than the amount of dry powder, which means *L/S* is less than 1. The aim was to investigate the effect of water on the carbonation rate during the transition from the dry to the aqueous phase.

Moreover, different concentrations of NaCl solution, including 1-molar and 2-molar, were utilized to study the effect of salinity compared to pure water on CO_2 mineralization. All aqueous samples were kept for 24 h before starting the experiment and dried after the experiment in the oven at 120 °C for 2 h. Other specified levels for the parameters are listed in Table 1.

Sequestration rate and carbonation efficiency calculations

Carbonation efficiency, sometimes referred to as carbonation conversion or degree of carbonation, is the primary response factor for assessing the quality of the carbonation process. To quantify the carbonation efficiency, the reactive alkaline extent, like Ca (Eqs. 12–16), in the sample was determined first (Kashim et al. 2020; Rahmani 2020; Ding et al. 2023).

$$\zeta_{Ca}(\%) = \frac{\left(\Delta W_{(1)} - \Delta W_{(0)}\right)_{CaCO_3}}{Ca_{unreacted}(\%)} \times \frac{M_{Ca}}{M_{CO_2}} \times 100 \tag{12}$$

$$Ca_{unreacted}(\%) = Ca_{total}(\%) - Ca_{reacted}(\%) \tag{13}$$

$$Ca_{total}(\%) = CaO(wt\%) \times \frac{M_{Ca}}{M_{CaO}} \tag{14}$$

$$Ca_{reacted}(\%) = \Delta W_{(0)} \times \frac{M_{Ca}}{M_{CO_2}} \tag{15}$$

$$(1),(2),(3),(4) \overset{yields}{\longrightarrow} \zeta_{Ca}(\%) = \frac{\left(\Delta W_{(1)} - \Delta W_{(0)}\right)_{CaCO_3}}{\left(CaO(wt\%) \times \frac{M_{CO_2}}{M_{CaO}}\right) - \left(\Delta W_{(0)}\right)_{CaCO_3}} \times 100 \tag{16}$$

Where ζ_{Ca} is the carbonation efficiency of Ca and $\left(\Delta W_{(1)} - \Delta W_{(0)}\right)_{CaCO_3}$ is the weight loss percentage

Table 1 Specified parameters in three phases of CO_2 mineralization of the Segamat basalt

Phase *	Run	Duration (min)	Particle size Group **	Temperature (°C)	Pressure (kPa)	L/S ratio	Salinity (molar)
Dry	D1	120	*P2*	60	200	0	-
	D2	120	*P2*	80	200	0	-
	D3	240	*P3*	80	200	0	-
	D4	180	*P1*	60	200	0	-
	D5	480	*P1*	60	200	0	-
	D6	180	*P1*	80	250	0	-
Transition	W1	180	*P1*	60	150	0.1	0
	SW1	180	*P1*	60	150	0.1	2
	SW2	90	*P1*	60	100	0.5	2
Aqueous	W2	90	*P1*	60	100	1	0
	SW3	90	*P1*	60	100	1	2
	SW4	90	*P1*	40	100	1	2
	SW5	30	*P1*	60	100	1	2
	SW6	90	*P2*	60	100	1	2
	SW7	90	*P3*	60	100	1	2
	SW8	60	*P1*	60	100	1	2
	SW9	90	*P1*	26	100	1	2
	SW10	90	*P1*	26	100	1	1

* Experiments with pure water are indicated by W, and SW indicates those with saline water

** The size distribution of each group is presented in section 3.1

difference between uncarbonated and carbonated samples in TGA within the specified temperature range related to the decomposition of calcite ($CaCO_3$) based on DTG analysis. $M_{Ca}$and M_{CO_2} are the molecular weight of calcium and carbon dioxide, respectively. The weight% of CaO in the raw material is also derived from XRF analysis. The calculation procedure for the efficiency of Mg and Fe is the same unless the weight loss related to the decomposition of each cation should be considered in its calculation (Eqs. 17, 18). In the calculation of Fe (Eq. 18), it is assumed that all the Fe in the basalt components can theoretically be released as Fe^{2+} in the dissolution phase.

$$\zeta_{Mg}(\%) = \frac{\left(\Delta W_{(1)} - \Delta W_{(0)}\right)_{MgCO_3}}{\left(MgO(wt\%) \times \frac{M_{CO_2}}{M_{MgO}}\right) - \left(\Delta W_{(0)}\right)_{MgCO_3}} \times 100 \quad (17)$$

$$\zeta_{Fe}(\%) = \frac{\left(\Delta W_{(1)} - \Delta W_{(0)}\right)_{FeCO_3}}{\left(Fe_2O_3(wt\%) \times \frac{2 \times M_{CO_2}}{M_{Fe_2O_3}}\right) - \left(\Delta W_{(0)}\right)_{FeCO_3}} \times 100 \quad (18)$$

In Eq. 19, the total carbonation efficiency (ζ_{total}) is calculated based on the average of cations efficiencies with respect to the molar fraction of each alkaline, i.e., m_{CaO}, m_{MgO}, and $m_{Fe_2O_3}$ (Eqs. 20–22).

$$\zeta_{total}(\%) = m_{CaO} \times \zeta_{Ca} + m_{MgO} \times \zeta_{Mg} + m_{Fe_2O_3} \times \zeta_{Fe} \quad (19)$$

$$m_{CaO} = \frac{CaO(wt\%)/M_{CaO}}{\left(\begin{array}{l} CaO(wt\%)/M_{CaO} + \\ MgO(wt\%)/M_{MgO} + \\ Fe_2O_3(wt\%)/M_{Fe_2O_3} \end{array}\right)} \quad (20)$$

$$m_{MgO} = \frac{MgO(wt\%)/M_{MgO}}{\left(\begin{array}{l} CaO(wt\%)/M_{CaO} + \\ MgO(wt\%)/M_{MgO} + \\ Fe_2O_3(wt\%)/M_{Fe_2O_3} \end{array}\right)} \quad (21)$$

$$m_{Fe_2O_3} = \frac{Fe_2O_3(wt\%)/M_{Fe_2O_3}}{\left(\begin{array}{l} CaO(wt\%)/M_{CaO} + \\ MgO(wt\%)/M_{MgO} + \\ Fe_2O_3(wt\%)/M_{Fe_2O_3} \end{array}\right)} \quad (22)$$

From Eq. 23, the CO_2 sequestration rate or CO_2 uptake is calculated based on the total weight loss between the specified temperature range:

$$R_{CO_2}(g/kg_{basalt}) = \left(\Delta W_{(150°C-950°C)} - \Delta W_{(0)}\right)_{total} \times 10 \quad (23)$$

Considering the TGA instrument's accuracy, the error range of CO_2 uptake is determined at ±2.5 g/kg_{basalt}.

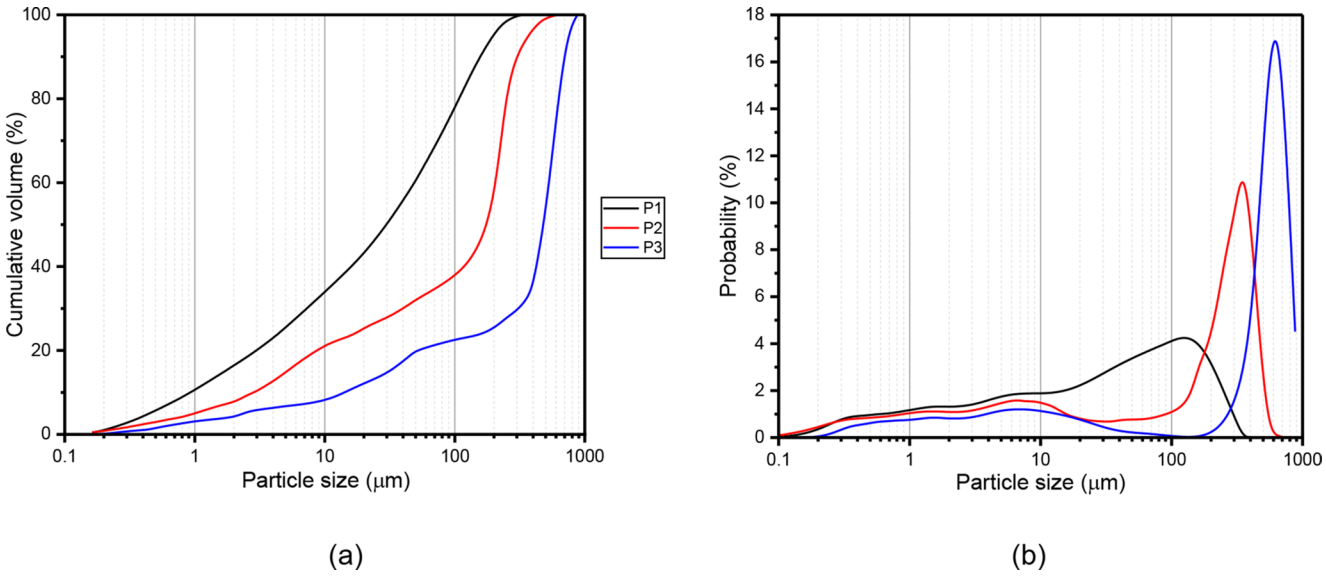

Fig. 3 (**a**) Cumulative volume and (**b**) the distribution of particle size for ground basalt sample

Table 2 Elemental composition of the Segamat basalt powder samples based on XRF analysis

Component	P1	P1	P2	P2	P2	P3	P3
SiO_2	39.36	38.58	38.37	38.58	39.83	39.91	39.61
Fe_2O_3	20.97	21.47	20.76	21.47	20.54	22.31	20.13
CaO	11.67	12.11	11.56	12.11	11.43	9.05	11.57
Al_2O_3	10.76	10.55	13.16	10.55	11.46	11.32	10.96
K_2O	6.61	6.38	6.60	6.38	6.54	7.38	7.02
MgO	4.70	4.76	4.71	4.76	4.72	4.11	4.77
TiO_2	2.46	2.01	2.12	2.01	1.69	1.91	1.93
P_2O_5	1.43	1.63	1.67	1.63	1.88	1.75	1.69
BaO	0.93	0.92	-	0.92	0.97	0.88	0.94
MnO	0.46	0.42	0.49	0.42	0.39	0.50	0.38
SrO	0.37	0.36	0.39	0.36	0.37	0.48	0.38
ZrO_2	0.17	0.06	0.07	0.06	0.08	0.18	0.05
Rb_2O	0.07	0.06	0.07	0.06	0.07	0.11	0.07

Results and discussion

Particle size distribution

The particle size analysis results are depicted in Fig. 3. Based on this analysis, the average particle sizes are 30, 175, and 480 μm for the P1, P2, and P3 groups, respectively. The P1 group has a wider range of distribution than the other two groups. However, nearly 90% of particles in P1 are below 150 μm, while this threshold is 300 μm and 700 μm for P2 and P3, respectively. Thus, P1, P2, and P3 are classified as fine, semi-fine, and coarse particles.

Elemental analysis

All XRF results listed in Table 2 demonstrate consistency with low fluctuations in the quantification of components across different particle size groups, aligning with XRF data from the literature for the Segamat basalt (Ayub et al. 2020). An average of 11.5% calcium oxide, along with 4.7% magnesium oxide and 21.1% iron oxide, indicates that the Segamat basalt is a suitable candidate for mineral carbonation purposes.

Crystal structure

The X-ray diffractograms obtained from all particle size groups display a consistent pattern with slight variations in major peaks (for uncarbonated samples), demonstrating that with sufficient care in sample preparation, the results remain reliable even for large particle sizes.

In Fig. 4, mineralogical analysis of the XRD patterns of the Segamat basalt is depicted with respect to XRF results, which is in agreement with the literature data (Ayub et al. 2020). From a geological point of view, the

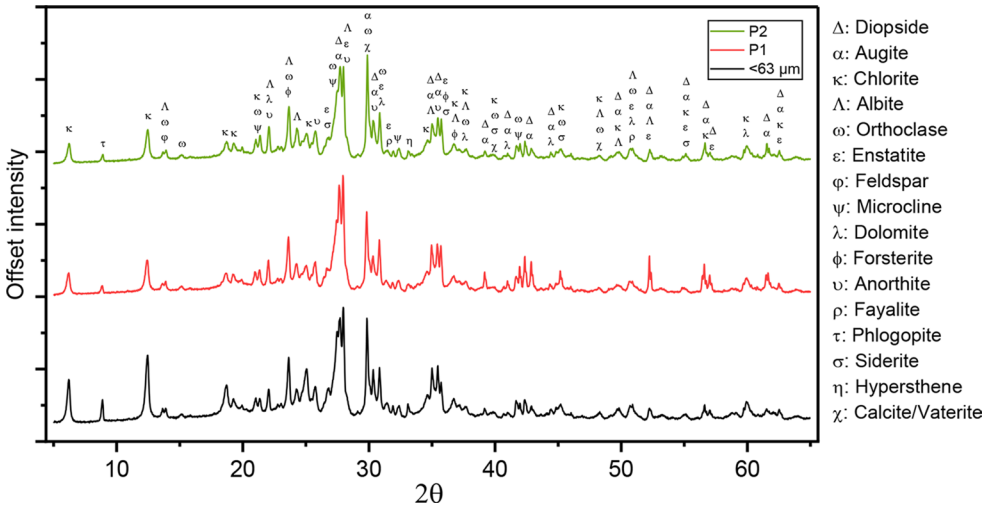

Fig. 4 X-ray Diffractogram and mineralogical identification for untreated Segamat basalt powder

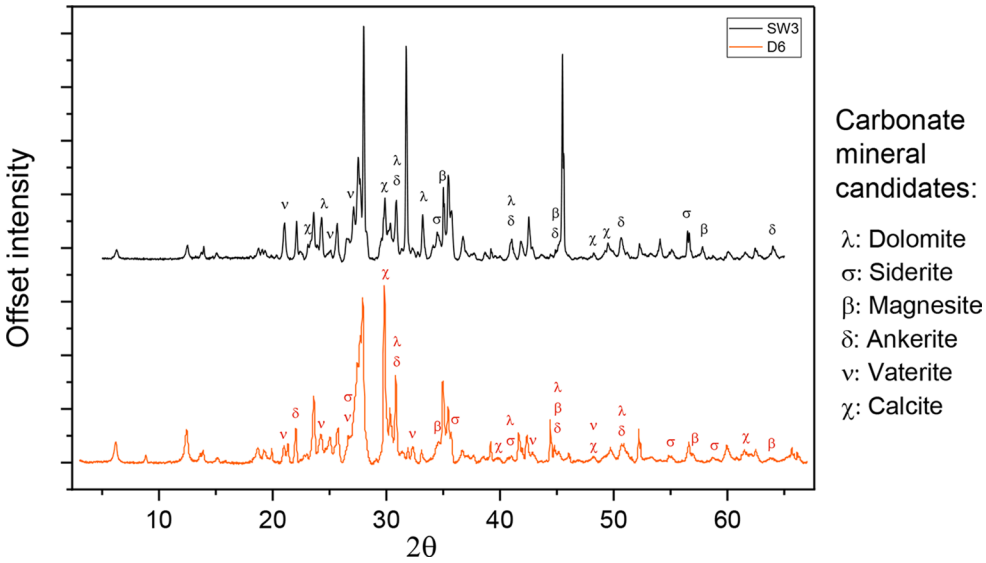

Fig. 5 Detecting possible carbonate candidates in XRD patterns of the dry and aqueous carbonated basalt samples

XRD patterns categorize the Segamat basalt as an ultramafic rock (<45 wt% silica) (Saleh et al. 2025) and present the existence of diopside ($Ca_{0.9}Mg_{0.9}Al_{0.2}K_{0.1}Si_{1.9}O_6$), augite ($CaMg_{0.75}Fe_{0.25}Si_2O_6$), and enstatite ($MgSiO_3$) from pyroxene group; forsterite ($Mg_{1.87}Fe_{0.13}SiO_4$) and fayalite (Fe_2SiO_4) from olivine group; orthoclase ($KAlSi_3O_8$) from feldspar group; albite ($NaAlSi_3O_8$) and anorthite ($CaAl_2Si_2O_8$) from plagioclase group. Chlorite ($Mg_{1.5}Fe_{0.2}Al_{0.6}SiO_6$) is also another important group that participates in basalt constituents.

Dolomite ($CaMg(CO_3)_2$), siderite ($FeCO_3$), and calcite/vaterite ($CaCO_3$) are three carbonate mineral candidates among ingredients of this basalt rock that fit well with the XRD pattern's peaks. Figure 5 shows the XRD patterns for the dry and aqueous carbonated samples with the best-achieved efficiencies (D6 and SW3). Based on the given patterns, the most probable carbonate minerals are dolomite, siderite, magnesite, ankerite, vaterite, and calcite. Further, the derivative of TGA provides supplementary clues from decomposition peaks to predict carbonate minerals and identifies the presence of the selected candidates in each phase of the experiments.

TGA-DTG analysis

Figure 6 compares the TGA and DTG between three uncarbonated, gas-solid, and aqueous carbonated samples. DTG analysis can effectively assist in investigating the existence of mineral carbonate candidates represented in Fig. 5 by detecting weight loss peaks based on the thermal decomposition characteristics of candidates.

Figure 6 (b) depicts DTG curves for uncarbonated and gas-solid samples consisting of two main peaks of weight loss. The first peak, starting from 450 °C to 640 °C, can potentially be ascribed to siderite thermal decomposition (Kusin et al. 2023). The second peak's range, starting at

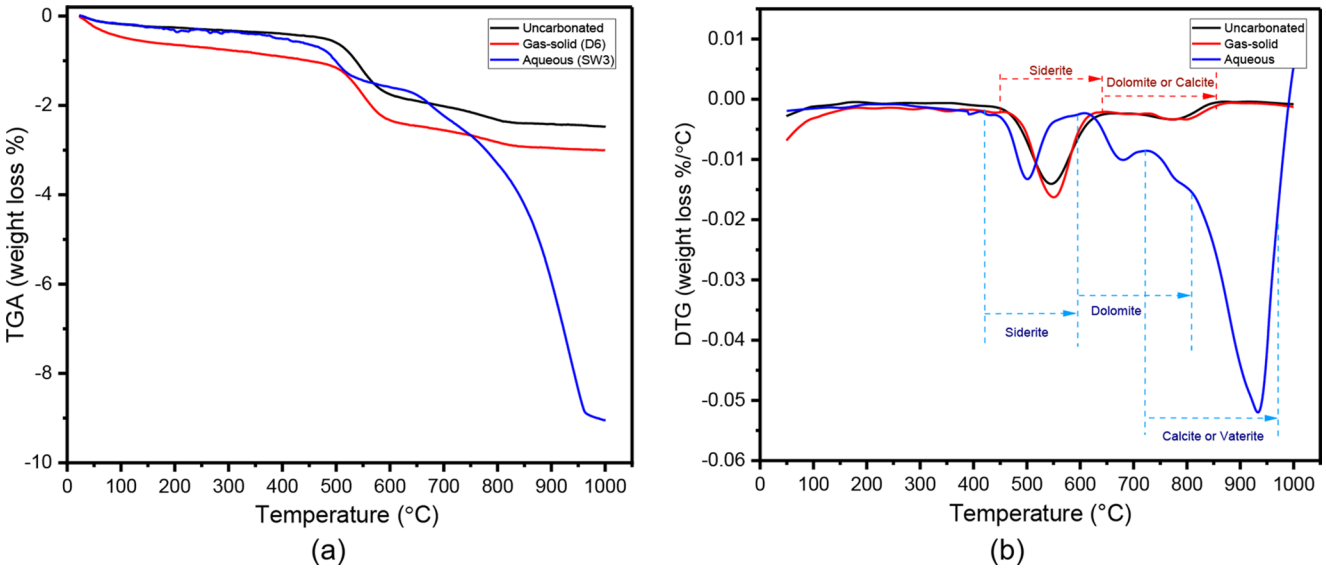

Fig. 6 Comparison between (**a**) TGA and (**b**) DTG curves for uncarbonated, gas-solid, and aqueous phases

640 °C and ending at 850 °C, fits well with the decomposition range of both dolomite and calcite (Qian et al. 2019; Kemp et al. 2022). However, a more detailed DTG in Fig. 9 shows that this peak consists of two extrema, similar to dolomite decomposition (Gabrovšek et al. 2006; Kemp et al. 2022).

For the aqueous phase, the DTG curve represents three major peaks, as indicated in Fig. 6 (b). Like the gas-solid phase, the first peak is related to siderite. The second peak, ranging from 600 °C to 810 °C, includes two steps of weight loss. The first step of weight loss, occurring between 600 °C and 720 °C, can be attributed to a secondary minor peak of siderite, as seen in other works (Alkac and Atalay 2008; Luo et al. 2016; Molahid et al. 2023; Ponomar 2023). Nevertheless, the secondary peak in siderite has a much smaller intensity compared to its primary peak of weight loss. Dolomite and ankerite are two other possible candidates, as both exhibit a two-step decomposition behavior in this temperature range (Gabrovšek et al. 2006; Ponomar 2023). However, ankerite's first step of weight loss is more intense than the second step (Ponomar 2023); in contrast, dolomite shows more weight loss in the second step (ranging from 720 °C to 810 °C), as noted in the literature (Gabrovšek et al. 2006; Kemp et al. 2022). Therefore, this weight loss peak is more similar to the pyrolytic characteristics of dolomite. The first step of this peak (between 600 °C and 720 °C) can be ascribed to the decomposition of $MgCO_3$. The last peak, ranging from 810 °C to 970 °C, is clearly the result of the thermal decomposition of $CaCO_3$, whether in the form of calcite, vaterite, or even amorphous calcium carbonate (Qian et al. 2019; Kemp et al. 2022; Wang et al. 2022; Bartels et al. 2024). The small difference in peak ranges between aqueous and gas-solid phases is interpreted as a result of the differing morphologies of carbonate minerals formed in each environment. These interpretations not only facilitate the investigation of the effects of parameters on the carbonation of each metal oxide but also enhance the accuracy of carbonation efficiency calculations.

FESEM

The characteristics of uncarbonated basaltic particles and the surface textures before the carbonation process have been illustrated in Fig. 7.

High-magnification images provided by the FESEM reveal that most carbonate minerals have grown irregularly on the surface of basalt particles. By comparing observations from Fig. 8 with other studies (Dabrowska et al. 2011; Gruszecka-Kosowska et al. 2017; Kumar and Shrivastava 2019b), it can be inferred that dolomite, siderite, and Ca-carbonate created multilayer flake structures with many porosities and agglomerated micro- and nano-crystals on the layers. It seems that in the low reaction conditions, they tend to form amorphous structures instead of major crystal structures of carbonates (Demény et al. 2016). Moreover, a significant volume of porosity on the particles' surface created a large surface area, which led to a considerable carbonation conversion rate. This can explain why the peak intensities in Fig. 5 did not show substantial increases compared to the XRD patterns of uncarbonated samples.

Effective parameters on the carbonation process

In this research, several parameters were studied in gas-solid transition, and aqueous phases to analyze their effect on the carbonation process in the low reaction environment. TGA

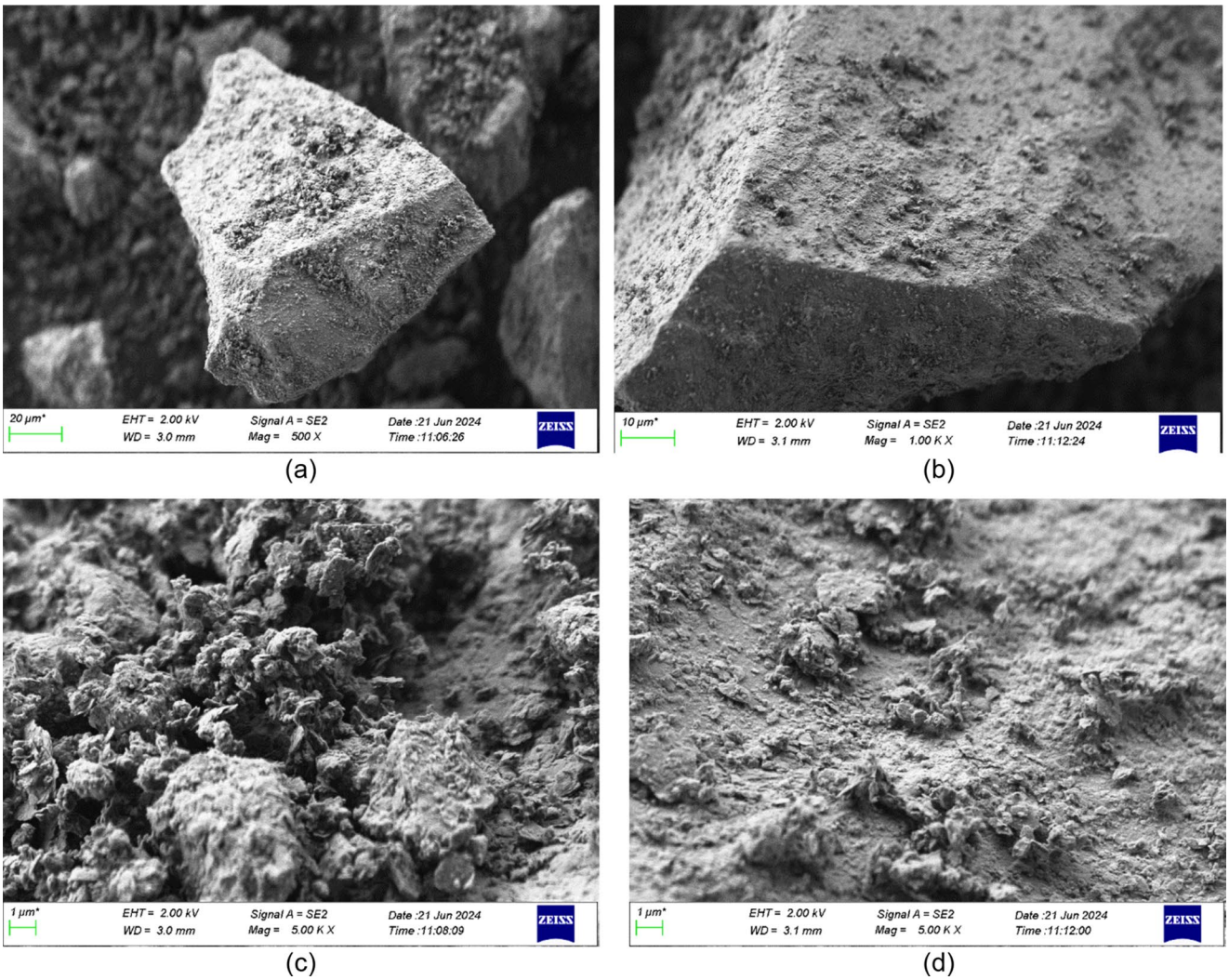

Fig. 7 (**a**) and (**b**) FESEM images of untreated basaltic particles, (**c**) and (**d**) a close snapshot of their surface textures

for the uncarbonated basalt sample shows 1.57–2.2% total weight loss, 1–1.64% of which belongs to the CO_2 extracted from the initial amount of siderite, and 0.52% is attributed to dolomite.

Table 3 listed the carbonation efficiency of each alkaline and CO_2 uptake for each experiment. The highest efficiency for calcium, at 71.36%, belongs to SW3. The maximum Mg efficiency, at 12.97%, occurred at SW8 in the aqueous phase. The best Fe efficiency was achieved in SW6 with 4.32%. Finally, the best total efficiency is also observed at SW3 with 28.65%. By calculating the efficiency for each reactive cation, the effect of parameters on each can be studied separately.

Gas-solid phase

The experiments of the dry (gas-solid) phase were conducted at 200–250 kPa pressure, a maximum temperature of 80 °C, and monitored for a duration of 120 to 480 min. As TGA curves in Fig. 9 show, the accelerated carbonation has been limited to the creation of siderite and dolomite, and no significant peak is observed for the decomposition of $CaCO_3$ related to calcite itself based on DTG analysis. This evidence proves that achieving calcite in gas-solid carbonation needs higher temperatures than 80 °C or considerably higher pressures than 250 kPa, and such prolonged experiments in a moderate reaction condition are not able to provide a feasible environment for the calcite creation even with an agitation mechanism. All gas-solid experiments only promoted the siderite to a very low extent.

Previous studies on the MC reveal that the creation of magnesite needs even higher pressure and requires hydromagnesite as an intermediate, which is out of reach in a dry process (Pasquier et al. 2014; Yadav and Mehra 2017). This fact becomes much more evident when we compare Mg-efficiency in all D1 to D6 experiments with SW1, where

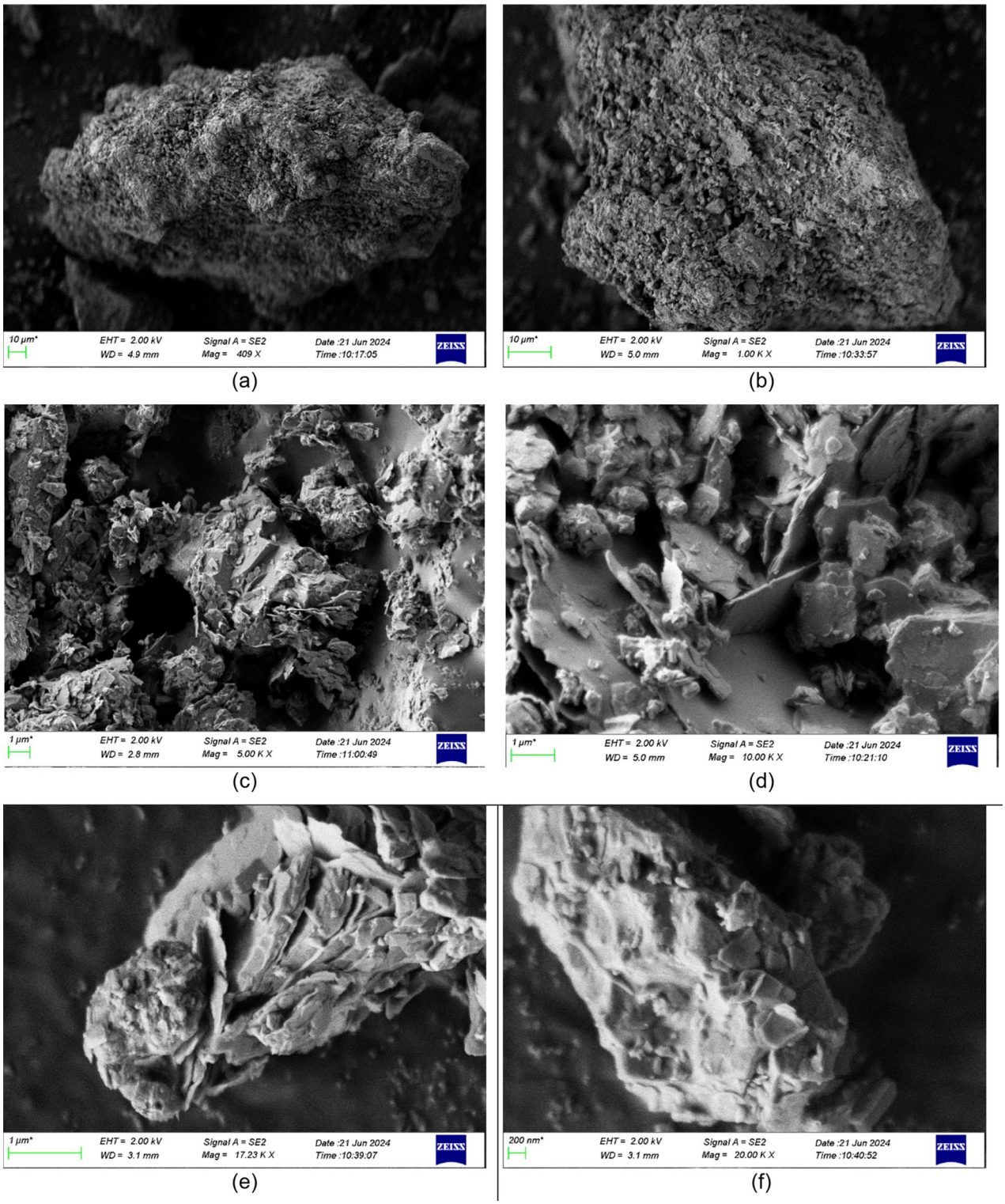

Fig. 8 (**a**) and (**b**) FESEM images of basalt particles after carbonation, (**c**) and (**d**) irregular and amorphous microstructures among the porosities and flakes on the silicate surface, (**e**) and (**f**) micro- and nano-agglomerated particles on the layers

Table 3 Carbonation efficiency and CO_2 uptake for each experiment of the Segamat basalt samples

Run	$\zeta_{Ca}(\%)$	$\zeta_{Mg}(\%)$	$\zeta_{Fe}(\%)$	$\zeta_{total}(\%)$	$R_{CO_2}(g/kg)$
D1	0	0	0.67	0.30	0
D2	0	0	0.27	0.12	0
D3	0	0	1.07	0.48	0.66
D4	0	0	1.56	0.70	0.80
D5	0	0	1.56	0.70	1.48
D6	0	0	2.25	1.02	2.01
W1	0	0	1.05	0.47	0
SW1	0.93	0.96	0.59	0.78	1.87
SW2	32.86	11.19	2.69	14.94	36.18
W2	4.07	3.30	1.83	2.91	0.80
SW3	71.36	11.35	3.13	28.65	70.32
SW4	60.73	11.72	1.38	24.21	59.37
SW5	68.42	10.73	1.04	26.56	65.24
SW6	62.85	7.22	4.32	25.39	62.15
SW7	67.46	7.86	1.55	25.88	63.54
SW8	64.56	12.97	2.07	26.11	64.05
SW9	65.89	10.08	2.32	26.11	64.06
SW10	27.04	4.93	7.04	13.62	32.67

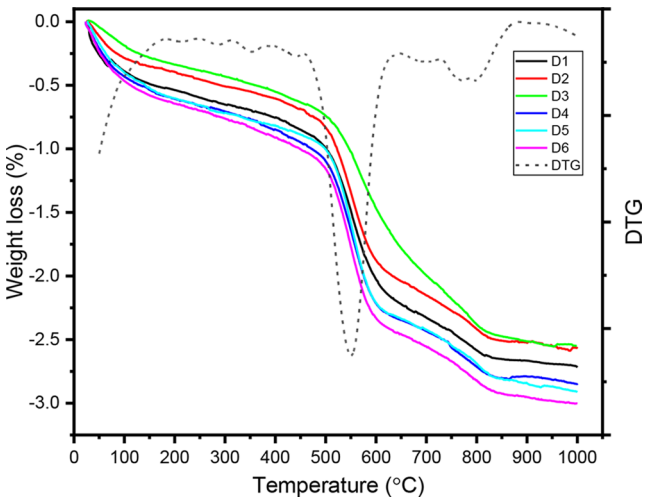

Fig. 9 TGA comparison between gas-solid carbonation experiments

adding a small amount of saline water initiates the creation of hydrate phases, which lead to the creation of Mg- and Ca-carbonate in a lower pressure. Overall, the results remind us that the efficiency of the gas-solid phase is not satisfactory in this range of temperature and pressure.

Salinity

Comparing the results of two aqueous experiments with different salinities of a 1-molar NaCl solution for SW10 and a 2-molar solution for SW9 with the results of W2, conducted in ultra-pure water, elucidates the crucial role of saline water for the carbonation reaction in low reaction conditions. Based on the TGA of run W2 in Fig. 10 (a), only 4.07% carbonation efficiency for Ca has been achieved by using ultra-pure water at 60 °C, 100 kPa, and $L/S=1$. In contrast, at a lower temperature (26 °C), the presence of 1-molar salinity resulted in a significant increase of up to 27.04% in Ca efficiency and 32.67 g CO_2 lockup per kg basalt powder in SW10. Eventually, proceeding to 2-molar salinity resulted in achieving a considerable 65.89% Ca efficiency and nearly 64 g CO_2 uptake per kg basalt in SW9. Even in the transition phase, both W1 and SW1 runs have a liquid-to-solid ratio of 0.1, but SW1 contains NaCl. The SW1 results in Table 3 depict more efficiency for Mg and Ca. This evidence demonstrates the significance of salinity in achieving a high degree of carbonation in a low-temperature, low-pressure environment. Despite Mg and Ca, Fe demonstrated a better performance in 1-molar salinity rather than 2-molar. A deeper and steeper swing in the DTG curve of SW10 over the temperature range of 400 °C to 600 °C compared to SW9 in Fig. 10 (b) affirms this inference. Although Fe-carbonation slightly retreats during the increase of salinity concentration, Ca^{2+}, conversely, leaps to higher efficiency with more acceleration during the salinity enhancement from 1 molar to 2 molar, as shown in Fig. 14 (a). In other words, higher salinity provides a more favorable environment for Ca^{2+} than its competitor, Fe^{2+}, in the carbonation reaction.

Liquid-to-solid ratio

Another important factor for the MC is the proportion of water to solid powder, which primarily leads to the formation of an intermediate hydration phase before carbonation. Figure 11 illustrates how CO_2 uptake has significantly increased by raising the L/S ratio. During the transition from

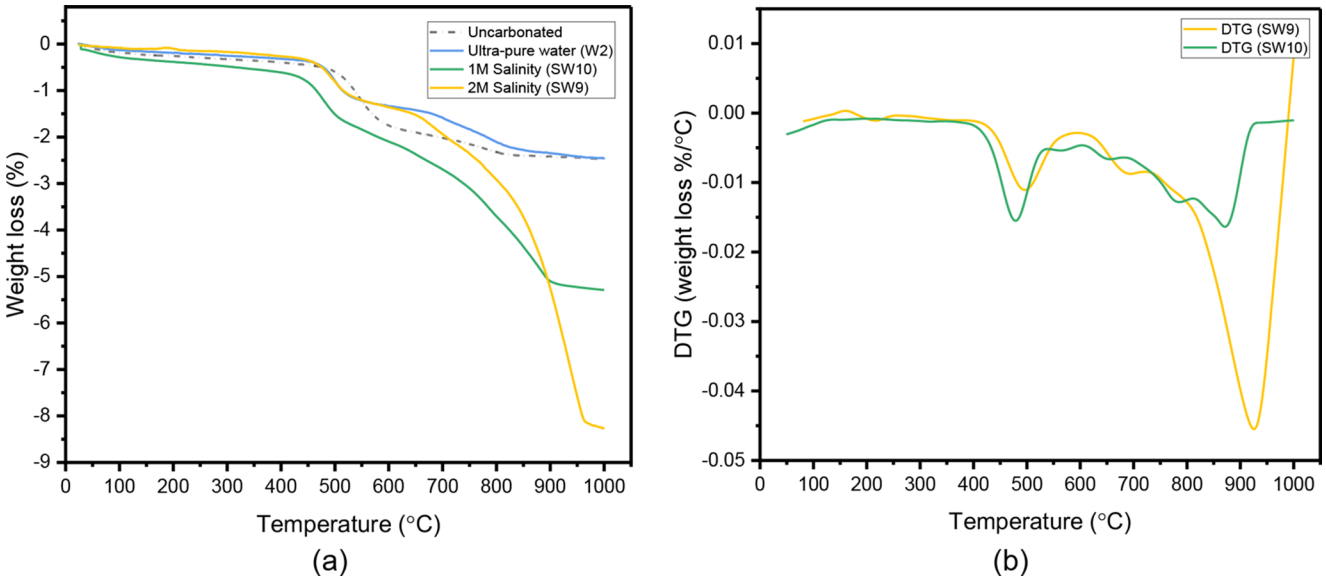

Fig. 10 Comparison between (**a**) TGA and (**b**) DTG for different salinity concentrations

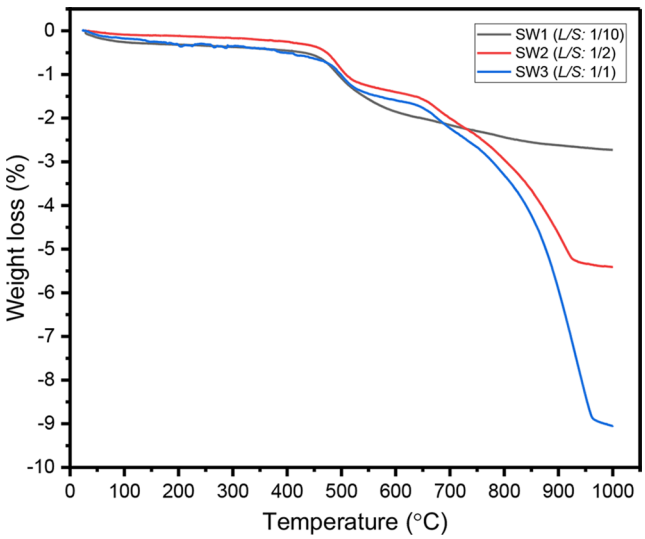

Fig. 11 TGA comparison between aqueous carbonation experiments using different *L/S* ratios

gas-solid to aqueous phase, two levels of *L/S* ratio were examined. Using an *L/S* ratio of 1/10, in which the sample is very close to the gas-solid phase, initiates the carbonation reaction, but to a very small extent. By raising the *L/S* ratio to 1/2 in run SW2, the carbonation reaction accelerates rapidly for Ca cation, as indicated in Fig. 14 (b). An increase in Mg efficiency is also observed, but it stops growing when the *L/S* ratio is increased to 1/1. There is no significant change in Fe efficiency based on *L/S* variation.

The TGA results in an overall 5.3% weight loss for SW2, corresponding to 36.18 g CO_2 lockup per kg of basalt. However, this sample agglomerated during the experiment, which may have hindered further carbonation. Finally, by using an *L/S* ratio of 1/1 in run SW3, a significant increase in sequestration is achieved, resulting in an 8.7% overall weight loss between 150 °C and 970 °C, which corresponds to a 70.32 g CO_2 lockup.

Temperature

A range from room temperature to 60 °C was investigated during the aqueous phase experiments. From the TGAs plotted in Fig. 12 (a) and comparing efficiencies in Fig. 14 (c), it is inferred that at 26 °C, carbonation slightly outperformed that at 40 °C. The decreasing *L/S* ratio can explain this issue due to the evaporation of moisture at 40 °C, resulting in less carbonation. Besides, this investigation proves that raising the temperature from room temperature to a degree less than 60 °C does not demonstrate a positive impact on MC. This finding is particularly significant, especially for pilot-scale MC projects involving large quantities, where energy consumption is a crucial factor that must be considered alongside process efficiency. Therefore, designing an MC project that works at ambient temperature and pressure can effectively move toward the net-zero emissions goal.

Reaction time

The effect of reaction time on the aqueous carbonation phase was studied in 30-, 60-, and 90 min. Based on the TGAs in Fig. 12 (b) and carbonation results in Fig. 14 (d), the efficiency runs in the 30-min and 60-min are very close to each other, and both have relatively low differences with the 90-min run. This comparison demonstrates that saline water creates a highly susceptible environment for the

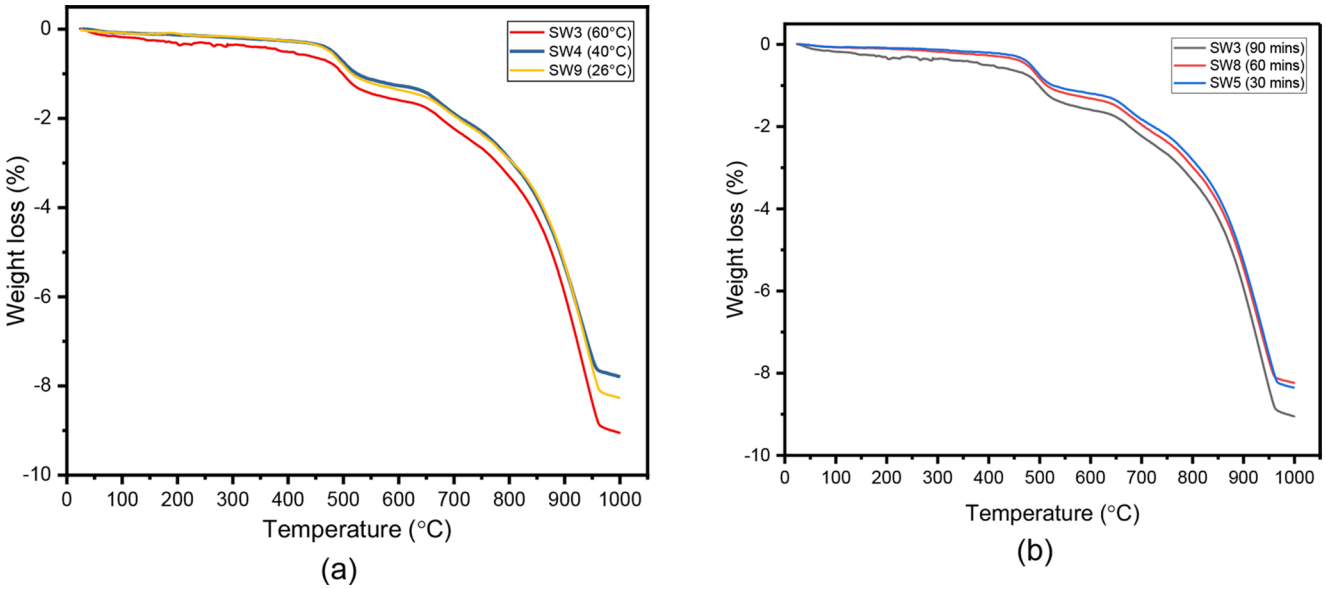

Fig. 12 TGA comparison between aqueous carbonation experiments (**a**) with different temperatures and (**b**) different durations

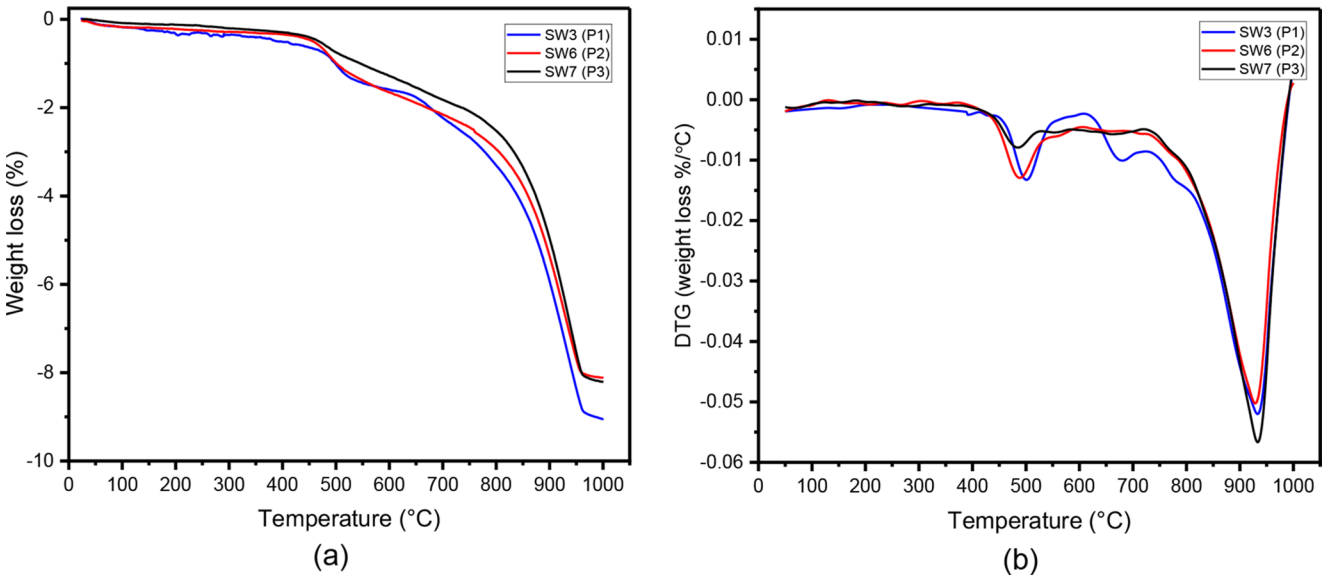

Fig. 13 Comparison between (**a**) TGA and (**b**) DTG for different particle size groups

carbonation reaction, which achieves high efficiency for Ca within the first 30 min of the MC process under low reaction conditions (i.e., SW5), resulting in a 65.24 g/kg sequestration rate.

Particle size

Figure 13 compares the TGA and DTG of three particle size groups in aqueous experiments, bringing two significant findings. First, contrary to most previous studies, this study demonstrates that carbonation for coarse particles is as feasible as for fine particles, even for such large particles in the range of 300 µm to 700 µm.

Second, as the particle size increases, less dolomite and more calcium carbonate are formed, as indicated by the DTGs in Fig. 13 (b). Figure 14 (e) also confirms this statement by decreasing Mg efficiency through growing particle size. This figure also indicates that the efficiency of Ca slightly increases at a large particle range (P3), while the efficiency of Fe decreases. This minor change may have originated from the use of P1 and P2 particle size groups in weight loss calculations for uncarbonated samples, which likely differ from those of P3. There is no sudden drop in total efficiency and the sequestration rate by increasing the particle size range. Thus, accelerated mineral carbonation is not limited to fine particle ranges. All parameters' effects

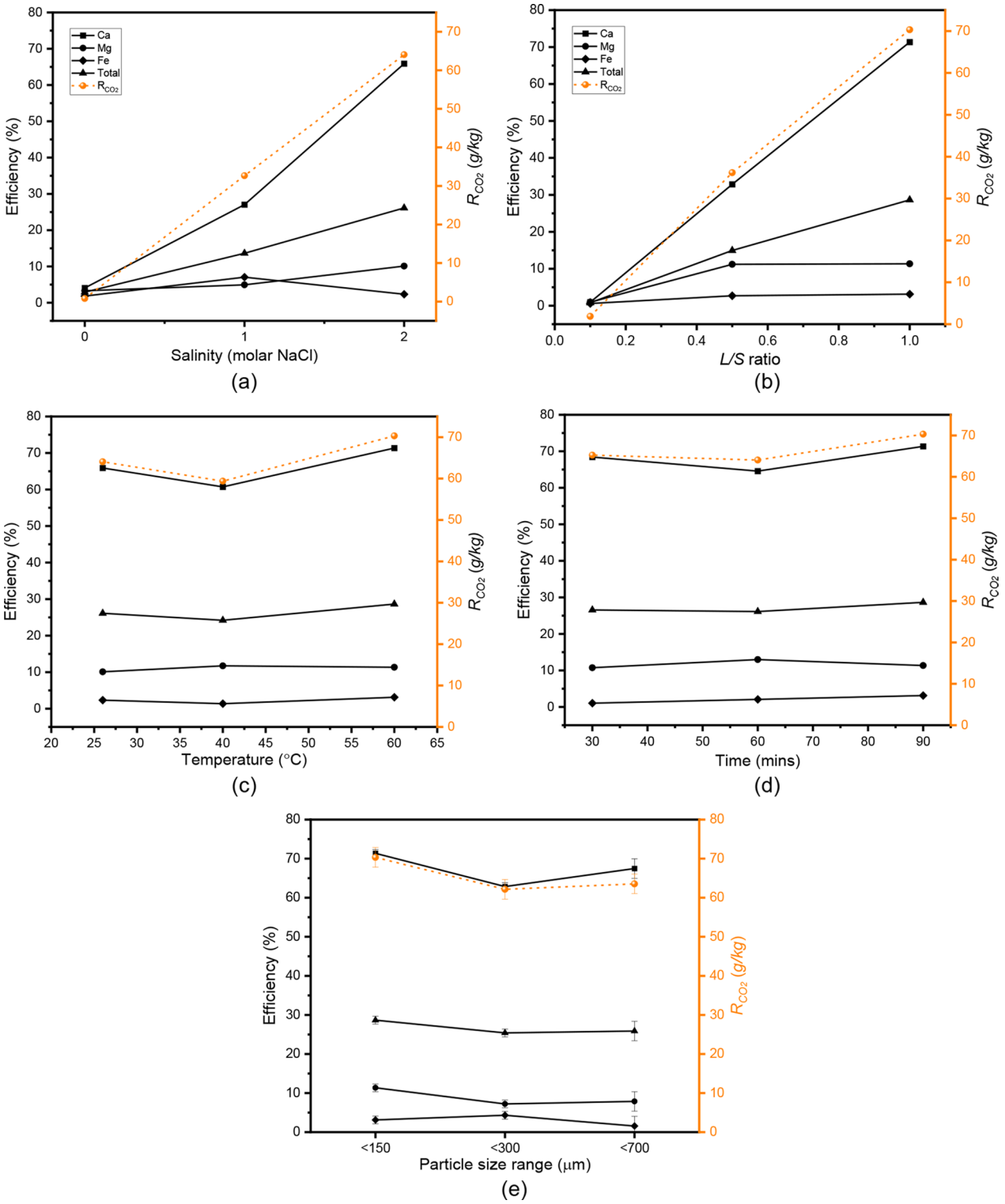

Fig. 14 Comparing efficiencies and carbon sequestration rate over each parameter changes

Table 4 Comparison of efficiencies and CO_2 uptake between the current study and other works

Ref.	Rock type (mineral group)	Primary constituents (wt%)	Conditions	Time	ζ_{total} (%)	R_{CO_2} (g/kg)
This study	basalt	(8.2% Ca, 2.8% Mg, 14.8% Fe^{2+})	1–2 M NaCl, *L/S*: 1, 26–60 °C, 1 bar, < 700 µm	30–90 min	14–29	33–70 (mostly affected by salinity)
(Zhou 2024)	Basalt (considering MgO and CaO contents of basalt only)	NA	Enhanced weathering, 25 °C, 1 bar, 50–500 µm,	1 yr	NA	4–74 (mostly affected by particle size)
(Goldberg et al. 2018)	Basalt	NA	Seawater, *L/S*: NA, 27 °C, 1 bar, < 60 µm	2 h	12	NA
(O'Connor et al. 2005)	Basalt (Anorthite, Augite, Magnetite, Olivine)	(6.7% Ca, 4.3% Mg, 6.7% Fe^{2+}	0.64 M $NaHCO_3$ & 1 M NaCl, *L/S*: 5.7, 185 °C, 150 bars, (80%) < 37 µm	60 min	Max 15	29-52.6
(O'Connor et al. 2005)	Augite (Pyroxene)	15.6% Ca, 6.9% Mg, 9.6% Fe^{2+}	0.64 M $NaHCO_3$ & 1 M NaCl, *L/S*: 5.7, 185 °C, 150 bars, (80%) < 37 µm	6 h	33	111
(O'Connor et al. 2005)	Forsterite (Olivine)	0.1% Ca, 27.9% Mg, 6.1% Fe^{2+}	0.64 M $NaHCO_3$ & 1 M NaCl, *L/S*: 5.7, 185 °C, 150 bars, (80%) < 37 µm	60 min	81	297
(O'Connor et al. 2005)	Fayalite (Olivine)	0.6% Ca, 0.3% Mg, 44.3% Fe^{2+}	0.64 M $NaHCO_3$ & 1 M NaCl, *L/S*: 5.7, 185 °C, 150 bars, (80%) < 75 µm	6 h	66	192
(O'Connor et al. 2005)	Anorthite (Feldspar)	10.3% Ca, 4.8% Mg, 3.1% Fe^{2+}	0.64 M $NaHCO_3$ & 1 M NaCl, *L/S*: 5.7, 185 °C, 150 bars, (80%) < 37 µm	6 h	9	19
(O'Connor et al. 2005)	Magnetite	0.6% Ca, 0.3% Mg, 21.9% Fe^{2+}	0.64 M $NaHCO_3$ & 1 M NaCl, *L/S*: 5.7, 185 °C, 150 bars, (80%) < 75 µm	6 h	8	15

on the efficiencies and carbon sequestration have been illustrated in Fig. 14. It should be noted that Figs. 14 (a) to (d) include data from those experiments conducted on the P1 particle size group, which has an error range of ±1%. This error range increases to ±2.5% for the P3 particle size group, as shown in Fig. 14 (e).

Field pilot of CO_2 uptake by Segamat basalt

Although basalt has not typically been considered a feedstock target for ex-situ MC purposes, Table 4 compares the findings of this research, which focuses solely on the aqueous phase, to existing literature. This comparison, which also includes the carbonation results, aims to provide a clear assessment of the efficiency achieved with respect to the mineral components of basalt. Table 4, a general overview of the results, confirms that the current achievements align well with an acceptable range, considering low environmental conditions and consistent efficiency in a broad particle size range and short reaction time. It seems that when a type of rock provides a comparative mixture of three major cations for carbonation, reaching high efficiencies is more complicated than those incorporating a single dominant divalent cation, such as forsterite (dominant in Mg^{2+}) and fayalite (dominant in Fe^{2+}).

Conclusion

This study comprehensively examined the ex-situ mineral carbonation of Segamat basalt, particularly during the transition from gas-solid to aqueous phase under low reaction conditions. The material characterization of Segamat basalt confirmed it as a suitable candidate for mineral carbonation due to its significant metal oxide content. Various experiments were conducted to understand the behavior of carbonate minerals during the carbonation process. The MC results underscored the limitations of gas-solid phase carbonation at moderate temperatures and pressures, with significant efficiency gains observed only upon transition to aqueous phases. Higher *L/S* ratios notably increased CO_2 uptake and overall carbonation efficiency, emphasizing the importance of water availability in promoting carbonation reactions. However, it is essential to note that the presence of saline water, particularly a 2-molar NaCl solution, plays a crucial role in significantly enhancing carbonation efficiency, especially for calcium, under low-temperature and low-pressure conditions. One of the key findings of this study was the investigation of particle size in the mineral carbonation process.

Contrary to previous studies focusing on fine particles, this research explored the feasibility of carbonation for larger particles in the range of 300 µm to 700 µm. The results showed that carbonation for coarse particles is as feasible as fine particles, providing valuable insights for

industrial applications where producing fine powder in large quantities can be challenging. Another notable finding was achieved by investigating the relationship between temperature and reaction duration. While the temperature rises to 60 °C did not considerably enhance carbonation efficiency, ambient conditions proved to gain an acceptable degree of carbonation. Furthermore, efficient carbonation was achieved within a 30-minute duration, indicating rapid reaction kinetics in the presence of saline water. By calculating the efficiency of each cation, the study of the parameters' effects on each mineral carbonate became more precise. Investigations suggested that calcium is the most reactive cation and $CaCO_3$ is the main downstream of MC in the low environment. The presence of salinity and an adequate L/S ratio indicated a key role, compared to the particle size of the feedstock, resulting in an almost 71% efficiency for calcium. Nevertheless, attaining high efficiencies for magnesium and iron is not possible and requires considerably higher temperatures and pressures.

Overall, the findings presented in this study contribute to the advancement of mineral carbonation technology and provide valuable insights into optimizing the MC process for practical CO_2 sequestration in low reaction conditions. Proving the feasibility of achieving an efficient carbonation process at room temperature and within a short reaction time implies the potential for energy-efficient industrial applications of MC under optimized conditions. This research serves as a stepping stone toward more efficient and sustainable carbon capture and storage technologies, as well as net-zero emissions targets.

Author contributions A.H.M. wrote the main manuscript. M.R.M. supervised the student, designed the experiment, equipment and funding acquisition. M.K.F. assisted the materials analysis. F.Y. contributed on student progress supervision and experiment. M.F.Z. assisted the TGA-DTG analysis. Z.F.A.H. assisted the FESEM analysis. H.K.H. contributed on the proposal and main idea contribution. O.R. worked on the manuscript improvement. A.A. worked on the writing checking and finalizing.

Funding Open access funding provided by The Ministry of Higher Education Malaysia and Universiti Malaya. The authors would like to thank Universiti Malaya (UM) for supporting this research through the "Impact Oriented Interdisciplinary Research Grant" with vote number IIRG002B-2022IISS.

Data availability Data is provided within the manuscript.

Declarations

Competing interests The authors declare no competing interests.

References

Alkac D, Atalay Ü (2008) Kinetics of thermal decomposition of Hekimhan–Deveci siderite ore samples. Int J Min Process 87:120–128

Ayub SA, Tsegab H, Rahmani O, Beiranvand Pour A (2020) Potential for CO2 mineral carbonation in the paleogene Segamat basalt of Malaysia. Minerals 10:1045

Bachu S, Bonijoly D, Bradshaw J et al (2007) CO2 storage capacity estimation: methodology and gaps. Int J Greenh Gas Control 1:430–443

Bartels MF, Miller QRS, Cao R et al (2024) Parts-per-million carbonate mineral quantification with thermogravimetric analysis–mass spectrometry. Anal Chem

Benson SM, Surles T (2006) Carbon dioxide capture and storage: an overview with emphasis on capture and storage in deep geological formations. Proc IEEE 94:1795–1805

Callow B, Falcon-Suarez I, Ahmed S, Matter J (2018) Assessing the carbon sequestration potential of basalt using X-ray micro-CT and rock mechanics. Int J Greenh Gas Control 70:146–156

Crippa M, Guizzardi D, Muntean M et al (2020) Fossil CO2 emissions of all world countries. Luxemb Eur Comm 1–244

Dabrowska DD, Muñoz O, Moreno F et al (2011) Scattering matrix measurements and light-scattering calculations of calcite particles. Atti Della Accad Peloritana Dei Pericolanti-Classe Di Sci Fis Mat E Nat 89

de Obeso JC, Awolayo AN, Nightingale MJ et al (2023) Experimental study on plagioclase dissolution rates at conditions relevant to mineral carbonation of seafloor basalts. Chem Geol 620:121348

Demény A, Németh P, Czuppon G et al (2016) Formation of amorphous calcium carbonate in caves and its implications for speleothem research. Sci Rep 6:39602

Dichicco MC, Laurita S, Paternoster M et al (2015) Serpentinite carbonation for CO2 sequestration in the southern Apennines: preliminary study. Eur. Geosci. UNION Gen. Assem. 2015 - Div. ENERGY, Resour. Environ. EGU 2015 76:477–486

Ding Z, Zhang X, Cheng T et al (2023) Unlocking high carbonation efficiency: direct CO2 mineralization with fly Ash and seawater. Chem Eng Sci 282:119349

Fagerlund J, Teir S, Nduagu E, Zevenhoven R (2009) Carbonation of magnesium silicate mineral using a pressurised gas/solid process. Energy Procedia 1:4907–4914

Gabrovšek R, Vuk T, Kaučič V (2006) Evaluation of the hydration of Portland cement containing various carbonates by means of thermal analysis. Acta Chim Slov 53:159–165

Gadikota G, Matter J, Kelemen P, Park AA (2014) Chemical and morphological changes during olivine carbonation for CO2 storage in the presence of NaCl and NaHCO3. Phys Chem Chem Phys 16:4679–4693. https://doi.org/10.1039/C3CP54903H

Garcia B, Beaumont V, Perfetti E et al (2010) Experiments and geochemical modelling of CO2 sequestration by olivine: potential, quantification. Appl Geochem 25:1383–1396. https://doi.org/10.1016/j.apgeochem.2010.06.009

Goldberg D, Aston L, Bonneville A et al (2018) Geological storage of CO2 in sub-seafloor basalt: the carbonsafe pre-feasibility study offshore Washington state and British Columbia. Energy Procedia 146:158–165. https://doi.org/10.1016/j.egypro.2018.07.020

Grover SPP, Baldock JA (2012) Carbon chemistry and mineralization of peat soils from the Australian alps. Eur J Soil Sci 63:129–140. https://doi.org/10.1111/j.1365-2389.2011.01424.x

Gruszecka-Kosowska A, Baran P, Wdowin M, Franus W (2017) Waste dolomite powder as an adsorbent of cd, Pb (II), and Zn from aqueous solutions. Environ Earth Sci 76:1–12

Gupta H, Fan L-S (2002) Carbonation – calcination cycle using high reactivity calcium oxide for carbon dioxide separation from flue gas. Ind Eng Chem Res 41:4035–4042

IEA (2023) World Energy Outlook 2023. Paris

IEA NZ (2021) Net zero by 2050. IEA, Paris

Kale KB, Raskar RY, Rane VH, Gaikwad AG (2012) Preparation and characterization of calcium silicate for CO2 sorption. Adsorpt Sci Technol 30:817–830

Kashim MZ, Tsegab H, Rahmani O et al (2020) Reaction mechanism of wollastonite in situ mineral carbonation for CO2 sequestration: effects of saline conditions, temperature, and pressure. ACS OMEGA 5:28942–28954. https://doi.org/10.1021/acsomega.0c02358

Kelemen PB, Matter J, Streit EE et al (2011) Rates and mechanisms of mineral carbonation in peridotite: natural processes and recipes for enhanced, in situ CO2 capture and storage. Annu Rev Earth Planet Sci 39:545–576

Kemp SJ, Lewis AL, Rushton JC (2022) Detection and quantification of low levels of carbonate mineral species using thermogravimetric-mass spectrometry to validate CO2 drawdown via enhanced rock weathering. Appl Geochem 146:105465

Kumar A, Shrivastava JP (2019a) Carbon capture induced changes in Deccan basalt: a mass-balance approach. Greenh GASES-SCIENCE Technol 9:1158–1180. https://doi.org/10.1002/ghg.1923

Kumar A, Shrivastava JP (2019b) Long-term CO2 capture-induced calcite crystallographic changes in Deccan basalt, India. Environ Earth Sci 78. https://doi.org/10.1007/s12665-019-8378-x

Kumar A, Shrivastava JP, Pathak V (2017) Mineral carbonation reactions under water-saturated, hydrothermal-like conditions and numerical simulations of CO2 sequestration in tholeiitic basalt of the Eastern Deccan volcanic province, India. Appl Geochem 84:87–104

Kusin FM, Hasan SNMS, Molahid VLM et al (2023) Carbon dioxide sequestration of iron ore mining waste under low-reaction condition of a direct mineral carbonation process. Environ Sci Pollut Res 30:22188–22210. https://doi.org/10.1007/s11356-022-23677-3

Kwon S, Fan M, DaCosta HFM, Russell AG (2011) Factors affecting the direct mineralization of CO2 with olivine. J Environ Sci 23:1233–1239. https://doi.org/10.1016/S1001-0742(10)60555-4

Li J, Jacobs AD, Hitch M (2019) Direct aqueous carbonation on olivine at a CO2 partial pressure of 6.5 mpa. Energy 173:902–910

Liu W, Su S, Xu K et al (2018) CO2 sequestration by direct gas–solid carbonation of fly Ash with steam addition. J Clean Prod 178:98–107

Liu D, Agarwal R, Li Y, Yang S (2019) Reactive transport modeling of mineral carbonation in unaltered and altered basalts during CO2 sequestration. Int J Greenh GAS Control 85:109–120. https://doi.org/10.1016/j.ijggc.2019.04.006

Liu D, Agarwal R, Liu F et al (2022) Modeling and assessment of CO2 geological storage in the Eastern Deccan basalt of India. Environ Sci Pollut Res 29:85465–85481. https://doi.org/10.1007/s11356-022-21757-y

Luo Y, He D (2021) Research status and future challenge for CO2 sequestration by mineral carbonation strategy using iron and steel slag. Environ Sci Pollut Res 28:49383–49409. https://doi.org/10.1007/s11356-021-15254-x

Luo YH, Zhu DQ, Pan J, Zhou XL (2016) Thermal decomposition behaviour and kinetics of Xinjiang siderite ore. Min Process Extr Metall 125:17–25

Marieni C, Voigt M, Clark DE et al (2021) Mineralization potential of water-dissolved CO2 and H2S injected into basalts as function of temperature: freshwater versus seawater. Int J Greenh GAS Control. https://doi.org/10.1016/j.ijggc.2021.103357. 109:

Matter JM, Broecker WS, Gislason SR et al (2011) The carbfix pilot Project–storing carbon dioxide in basalt. Energy Procedia 4:5579–5585

Mazzotti M, Carlos Abanades J, Allam R et al (2005) Mineral carbonation and industrial uses of carbon dioxide

Molahid VLM, Kusin FM, Hasan SNMS (2023) Mineralogical and chemical characterization of mining waste and utilization for carbon sequestration through mineral carbonation. Environ Geochem Health. https://doi.org/10.1007/s10653-023-01513-y

Montes-Hernandez G, Chiriac R, Toche F, Renard F (2012) Gas–solid carbonation of Ca (OH) 2 and CaO particles under non-isothermal and isothermal conditions by using a thermogravimetric analyzer: implications for CO2 capture. Int J Greenh Gas Control 11:172–180

O'Connor WK, Dahlin DC, Rush GE et al (2005) Aqueous mineral carbonation. Final Report–DOE/ARC-TR-04-002

Park H, Han J, Lee J et al (2016) Comparison of two processes forming CaCO3 precipitates by electrolysis. Energies 9:1052. https://doi.org/10.3390/en9121052

Pasquier L-C, Mercier G, Blais J-F et al (2014) Parameters optimization for direct flue gas CO2 capture and sequestration by aqueous mineral carbonation using activated serpentinite based mining residue. Appl Geochem 50:66–73

Ponomar V (2023) Crystal structures and magnetic properties of spinel ferrites synthesized from natural Fe–Mg–Ca carbonates. Mater Res Bull 158:112068

Qian H, Kai W, Hongde X (2019) A novel perspective of dolomite decomposition: elementary reactions analysis by thermogravimetric mass spectrometry. Thermochim Acta 676:47–51

Rafiee A, Khalilpour KR, Milani D, Panahi M (2018) Trends in CO2 conversion and utilization: A review from process systems perspective. J Environ Chem Eng 6:5771–5794

Rahmani O (2020) An experimental study of accelerated mineral carbonation of industrial waste red gypsum for CO2 sequestration. J CO2 Util 35:265–271

Rahmani O, Highfield J, Junin R et al (2016) Experimental investigation and simplistic geochemical modeling of CO2 mineral carbonation using the Mount Tawai peridotite. Molecules 21:353

Rahmanihanzaki M, Hemmati A (2022) A review of mineral carbonation by alkaline solidwaste. Int J Greenh GAS Control. https://doi.org/10.1016/j.ijggc.2022.103798. 121:

Reynes JF, Mercier G, Blais J-F, Pasquier L-C (2021) Feasibility of a mineral carbonation technique using Iron-Silicate mining waste by direct flue gas CO2 capture and cation complexation using 2,2'-Bipyridine. Minerals 11. https://doi.org/10.3390/min11040343

Ritchie H, Roser M, Rosado P (2020) CO_2 and greenhouse gas emissions. Our world data

Romanov V, Soong Y, Carney C et al (2015) Mineralization of carbon dioxide: A literature review. CHEMBIOENG Rev 2:231–256. https://doi.org/10.1002/cben.201500002

Saleh MA, Ryan MP, Trusler JPM, Krevor S (2025) The interfacial processes controlling carbon dioxide mineralisation in magnesium and calcium silicates. Fuel 380:132969

Shi C, Li Y, Zhang J et al (2016) Performance enhancement of recycled concrete aggregate–a review. J Clean Prod 112:466–472

Snaebjornsdottir SO, Oelkers EH, Mesfin K et al (2017) The chemistry and saturation States of subsurface fluids during the in situ

mineralisation of CO2 and H2S at the carbfix site in SW-Iceland. Int J Greenh GAS Control 58:87–102. https://doi.org/10.1016/j.ijggc.2017.01.007

Tam VWY, Butera A, Le KN (2016) Carbon-conditioned recycled aggregate in concrete production. J Clean Prod 133:672–680

Tan W-L, Tan H-F, Ahmad AL, Leo CP (2021) Carbon dioxide conversion into calcium carbonate nanoparticles using membrane gas absorption. J CO2 Util 48. https://doi.org/10.1016/j.jcou.2021.101533

Wang F, Dreisinger D (2023) Enhanced CO2 mineralization and selective critical metal extraction from olivine and laterites. Sep Purif Technol. https://doi.org/10.1016/j.seppur.2023.124268. 321:

Wang WW, Wang SZ, Liu Q et al (2022) Study on the efficacy of amorphous calcium carbonate as a consolidant for calcareous matrix. Herit Sci 10. https://doi.org/10.1186/s40494-022-00804-4

Wells RK, Xiong W, Giammar D, Skemer P (2017) Dissolution and surface roughening of Columbia river flood basalt at geologic carbon sequestration conditions. Chem Geol 467:100–109. https://doi.org/10.1016/j.chemgeo.2017.07.028

Werner M, Hariharan SB, Bortolan AV et al (2013) Carbonation of activated serpentine for direct flue gas mineralization. GHGT-11 37:5929–5937

Yadav S, Mehra A (2017) Experimental study of dissolution of minerals and CO2 sequestration in steel slag. Waste Manag 64:348–357. https://doi.org/10.1016/j.wasman.2017.03.032

Yadav S, Mehra A (2019) Mathematical modelling and experimental study of carbonation of wollastonite in the aqueous media. J CO2 Util 31:181–191. https://doi.org/10.1016/j.jcou.2019.03.013

Yadav S, Mehra A (2021) A review on ex situ mineral carbonation. Environ Sci Pollut Res 28:12202–12231

Yusoff Afauzan, Hasnan H, kamal, Roselee M, hatta et al (2025) The potential of CO2 sequestration from basaltic rock in Peninsular Malaysia. Sains Malaysiana 54:3483–3493

Zhou Q (2024) Potential CO2 capture via enhanced weathering by basaltic sand spreading on golf courses in the US. Int J Greenh Gas Control 131:104032